Journal of Catalysis 257 (2008) 108–116

Contents lists available at ScienceDirect

Journal of Catalysis

www.elsevier.com/locate/jcat

Deactivation behavior of Pd-based SBA-15 mesoporous silica catalysts for the catalytic combustion of methane

Fengxiang Yin, Shengfu Ji *, Pingyi Wu, Fuzhen Zhao, Chengyue Li *

State Key Laboratory of Chemical Resource Engineering, Beijing University of Chemical Technology, 15 Beisanhuan Dong Road, P.O. Box 35, Beijing 100029, China

ARTICLE INFO

Article history:
Received 18 March 2008
Revised 15 April 2008
Accepted 16 April 2008
Available online 22 May 2008

Keywords:
Pd-based catalysts
Deactivation
SBA-15 mesoporous silica
X-ray powder diffraction
X-ray photoelectron spectroscopy
Temperature-programmed reduction

ABSTRACT

A series of Pd/SBA-15 and Pd/5% $Ce_{1-x}Zr_xO_2$/SBA-15 ($x = 0$–1) catalysts with Pd content ranging from 0.05% to 1% were prepared. The activity and stability of the catalysts for the combustion of methane were evaluated. The catalysts were characterized by X-ray diffraction (XRD), N_2 adsorption–desorption, CO chemisorption, transmission electron microscopy (TEM), X-ray photoelectron spectroscopy (XPS), and temperature-programmed reduction (TPR). Deactivation behavior of the catalysts for the catalytic combustion of methane was investigated. The results show that all of the catalysts retained the SBA-15 mesoporous structure, with PdO and $Ce_{1-x}Zr_xO_2$ being confined in the channels. It is proposed that deactivation of the catalysts is associated with accumulation of Pd^0, which cannot be efficiently reoxidized to PdO or PdO_2, due to the limited oxygen-transfer ability of the catalysts. The incorporation of the ZrO_2 as a promoter leads to an increase in the oxygen storage capacity and oxygen mobility of the catalysts, which in turn increases the rate of oxidation of Pd^0 and mitigates deactivation of the catalyst.

1. Introduction

Catalytic combustion of methane has been found to be more environmentally friendly than conventional flame combustion due to lower emissions of NO_x, CO, and unburned hydrocarbons as well as higher energy efficiency, and thus it has attracted increasing attention in recent years [1,2]. In addition, catalytic combustion of lean methane gas to abate methane emission from natural gas combustion devices or engines also has wide-ranging applications [2]. Supported palladium catalysts have been shown to have excellent activity toward methane oxidation, and PdO is generally considered the active species [3–5]. Of the different supports used for palladium, alumina has been reported to give the most active catalysts for methane combustion and has been studied extensively [1,2,6]; however, its poor durability hinders the development of viable catalytic combustors [2]. Various reasons have been suggested for the rapid deactivation of such Pd/Al_2O_3 catalysts; for example, it has been reported that deactivation results mainly from the sintering of γ-alumina [7] and the transformation of PdO → Pd [8], whereas Ozawa et al. [9,10] concluded that PdO/Al_2O_3 catalysts are rapidly deactivated due to the transformation of PdO to metallic Pd and more slowly deactivated due to the growth of PdO particles. Euzen et al. [11] have suggested that the deactivation of PdO/Al_2O_3 catalysts is due mainly to the transformation of PdO → Pd. Based on the general consensus in the literature, it can be concluded that catalyst stability can be increased by increasing the stability of the support, retarding the transformation of PdO → Pd, and suppressing the growth of PdO particles.

It is well known that ceria is an effective promoter for noble metal-based combustion catalysts, especially Pd/Al_2O_3 catalysts, and that ceria acts both as a phase-stabilizer for γ-alumina and to increase the dispersion and stability of the active form of the metal by means of a strong metal–support interaction [12,13]. But at high reaction temperatures, ceria is readily sintered, resulting in deactivation of the catalyst. It has been reported that formation of a solid solution by adding ZrO_2 to ceria leads to improved oxygen storage capacity (OSC), redox properties, and thermal resistance and to better catalytic activity at lower temperatures. Consequently, CeO_2–ZrO_2 solid solutions are widely used in three-way catalysts for treating automobile exhaust gas [14,15]. Although ZrO_2-based supports are stable at high temperature, they have the drawbacks of high cost and relatively low surface area [16,17]. Recently, mesoporous silica SBA-15 [18,19], which has a highly ordered hexagonal structure with high surface area (600–1000 $m^2\,g^{-1}$), adjustable pore sizes of 4.6–30 nm, and wall thickness of 3.1–6.4 nm, has attracted wide attention as a new material for catalysts and catalyst supports. Pd-based catalysts supported on SBA-15 have been reported to exhibit excellent activity both for the catalytic combustion of methane [20,21] and for Heck reactions [22,23], which has been attributed to the high dispersion of Pd within the channels of SBA-15. The influence of solvents on the formation of metal and its oxide nanoparticles in SBA-15 also has been investigated [24].

Before these catalysts can be considered for actual practical applications, their long-term stability must be evaluated. No such

* Corresponding authors. Fax: +86 10 64419619.
E-mail addresses: jisf@mail.buct.edu.cn (S. Ji), licy@mail.buct.edu.cn (C. Li).

0021-9517/$ – see front matter
doi:10.1016/j.jcat.2008.04.010

study has been reported to date, however. In the present work, a series of catalysts with varying Pd content, based on SBA-15 as the support and $Ce_{1-x}Zr_xO_2$ as the promoter, were prepared by the impregnation method, and their catalytic activity and stability during lean-methane combustion were investigated. The main goal was to explore the deactivation behavior of the catalysts for the complete oxidation of methane at low temperature.

2. Experimental

2.1. Catalyst preparation

SBA-15 was prepared as described previously [18]. In brief, 4 g of triblock poly (ethylene oxide)–poly(propylene oxide)–poly(ethylene oxide) ($EO_{20}PO_{70}EO_{20}$, M = 5800) was added to a mixture of 90 ml of deionized H_2O and 60 g of HCl (4 M), and stirred at 40 °C for 2 h. Then 8.5 g of tetraethyl orthosilicate (TEOS) was slowly added, and the mixture was stirred for another 22 h. The gel mixture was transferred to Teflon bottles and aged at 100 °C for 24 h under static conditions. After aging, the resulting solid was filtered, washed with deionized water until neutral, dried at room temperature, and finally calcined in flowing air at 500 °C for 6 h to remove the organic template.

The Pd/SBA-15 samples were prepared by the impregnation method using an aqueous solution of $Pd(NO_3)_2$. The 5% $Ce_{1-x}Zr_xO_2$/SBA-15 ($x = 0$–1) samples were prepared by coimpregnation of pure SBA-15 with a mixed aqueous solution of Ce and Zr nitrates. The Pd/5% $Ce_{1-x}Zr_xO_2$/SBA-15 samples were prepared by subsequent impregnation of these materials with an aqueous solution of $Pd(NO_3)_2$. The Pd content was varied from 0.1 to 1 wt%. All catalyst samples were dried at room temperature and then calcined in air at 500 °C for 4 h.

2.2. Characterization

XRD patterns were obtained on a Rigaku D/Max 2500 VB2+/PC diffractometer using Cu$K\alpha$ radiation with the following operating parameters: 200 mA, 40 kV, 2θ scanning from 10° to 90° for wide-angle XRD and 50 mA, 40 kV, 2θ scanning from 0.7° to 5° for low-angle XRD. N_2 sorption isotherms were obtained at liquid nitrogen temperature using a Thermo Electron Sorptomatic 1990 instrument. Before each analysis, the sample was degassed for 5 h at 250 °C under vacuum. BET and BJH analysis were used to determine the surface area and pore size distribution, respectively, of the samples. TEM images were obtained using a JEM2010 microscope operated at 200 kV. XPS experiments were carried out on an Thermo Electron Escalab250 instrument using Al$K\alpha$ as the exciting radiation at a constant pass energy of 50 eV. Binding energies were calibrated using the carbon present as a contaminant (C1s = 285.0 eV). The surface atomic compositions of all samples were calculated from photoelectron peak areas for each element after correction for instrument parameters.

The TPR experiments were performed using a Thermo Electron TPD/R/O 1100 series catalytic surface analyzer equipped with a thermal conductivity detector. The samples were heated under N_2 to 400 °C at a rate of 20 °C/min, then cooled in flowing N_2 to room temperature, and finally reduced with 5 vol% H_2/N_2 mixtures by heating to 900 °C at a rate of 20 °C/min. Water produced by sample reduction was condensed in a cold trap before reaching the detector. Only H_2 was detected in the outlet gas, confirming the effectiveness of the cold trap.

Pd dispersion, Pd surface area, and Pd crystallite size were evaluated by pulse chemisorption measurements with a Thermo Electron TPD/R/O 1100 series catalytic surface analyzer at 25 °C using CO as probe molecules. Before the chemisorption measurements, the catalyst samples were treated at 500 °C in a hydrogen flow for 2 h. A CO/Pd ratio of 1 was assumed for the Pd dispersion calculation.

2.3. Catalytic activity and stability

Catalytic activity evaluation and stability tests were carried out in a quartz microreactor (8 mm i.d., 300 mm long) at atmospheric pressure under steady-state conditions. The catalysts were pressed into tablets and then crushed and sieved to 60–80 mesh. A 0.1-g catalyst sample was loaded into the reactor for each run. A gas mixture of 2 vol% CH_4 in air with a gas hourly space velocity (GHSV) of 6000 ml g^{-1} h^{-1} was used to choose the catalysts to study for deactivation behavior and to carry out stability tests. A series of preliminary experiments was carried out to check for the lack of mass- and heat-transfer limitations. On testing two different catalyst loadings of 0.1 and 0.2 g and seven different GHSVs from 6000 to 72,000 ml g^{-1} h^{-1}, the influence of external mass transfer was found to be negligible at a GHSV > 36,000 ml g^{-1} h^{-1}. Internal mass and heat transfer limitations also were ruled based on the results of experiments with four different particle sizes (20–40, 40–60, 60–80, and 80–100 mesh) and two different temperatures (400 and 450 °C), as shown in Fig. S1 in the supplementary material. Thus, the intrinsic activity and activation energy of the catalysts can be obtained under our experimental conditions with particle sizes of 60–80 mesh and GHSV of 72,000 ml g^{-1} h^{-1}. The outlet products were measured by a gas chromatograph with a thermal conductivity detector (Beijing East and West Electronics Institute, GC-4000A). The reaction temperature was controlled with a K-type thermocouple placed in the vicinity of the catalytic bed. In every case, carbon dioxide and water were the only reaction products detected throughout the entire experiment. The stability tests for all samples were carried out at 450 °C. To confirm the repeatability of the data, the repeat runs were implemented for the study of intrinsic activity. Tests were considered valid when carbon balance was between 95% and 105%. The turnover frequency (TOF), defined as the number of reactant molecules converted to products per surface metal atom, was calculated based on the data from pulse chemisorption measurements using CO.

3. Results

3.1. Catalyst activity

The effect of Pd loading content on the observed activities of the Pd/SBA-15 catalysts was studied. The results of observed activity evaluation for Pd/SBA-15 catalysts are shown in Fig. S2 in the supplementary material. These are the temperatures at which conversion of 10%, 50%, and 90%, respectively, were obtained. The values of T_{10}, T_{50}, and T_{90} are listed in Table 1. The results of physicochemical properties and CO chemisorption measurements of the samples are listed in Table 2. It is shown that for the Pd/SBA-15, the observed activity of the catalyst increased substantially with an increase in Pd content from 0.05% to 0.5%, with a more modest increase with further increasing Pd content up to 1%. The TOF of the 0.5% Pd/SBA-15 catalyst was 13.2×10^{-3} s^{-1} at 450 °C, as reported in Table 2.

Because the catalyst exhibited only a marginal increase in observed activity when the Pd content was increased from 0.5% to 1%, the catalysts with a Pd loading of 0.5% were used to study the effect of CeO_2, ZrO_2, and Ce–Zr mixed oxides as promoters of catalyst performance. Fig. S3 in the supplementary material shows the observed activities of the 0.5% Pd/$Ce_{1-x}Zr_xO_2$/SBA-15 ($x = 0$, 0.5, 1) catalysts with different $Ce_{1-x}Zr_xO_2$ contents. It can be seen that when CeO_2, $Ce_{0.5}Zr_{0.5}O_2$, or ZrO_2 was used as a promoter, the catalyst had a maximum observed activity at a promoter loading of 5%. The TOF of the 0.5% Pd/$Ce_{1-x}Zr_xO_2$/SBA-15 ($x = 0$, 0.5, 1) catalyst

Table 1
Values of T_{10}, T_{50} and T_{90} for Pd/SBA-15 and 0.5% Pd/5% $Ce_{1-x}Zr_xO_2$/SBA-15 catalysts with different Pd loadings

Catalysts	T_{10} (°C)							T_{50} (°C)							T_{90} (°C)						
	%Pd							%Pd							%Pd						
	0.05	0.1	0.15	0.25	0.5	0.75	1.0	0.05	0.1	0.15	0.25	0.5	0.75	1.0	0.05	0.1	0.15	0.25	0.5	0.75	1.0
Pd/SBA-15	399	293	285	281	278	276	275	417	341	331	326	320	318	317	–	391	375	368	362	359	354
Pd/5% CeO_2/SBA-15	342	318	307	289	284	280	295	389	371	362	347	342	339	351	–	447	434	416	406	398	419
Pd/5% $Ce_{0.5}Zr_{0.5}O_2$/SBA-15	305	292	282	278	270	268	277	368	354	346	330	324	318	330	425	412	395	375	367	360	375
Pd/5% ZrO_2/SBA-15	285	275	270	265	262	259	263	350	329	324	322	317	314	322	399	369	365	363	352	352	364

Table 2
The results of physiochemical properties and CO chemisorption measurements of the samples

Samples	XRD measurements				N_2 adsorption–desorption measurements						CO chemisorption measurements							
	PdO (nm)		CeO_2 (nm)		S_{BET} ($m^2\,g^{-1}$)		V_P ($cm^3\,g^{-1}$)		D_{BJH} (nm)		n Pd (μmol $Pd\,g^{-1}_{catalyst}$)		Pd dispersion (%)		Pd crystallite size (nm)		TOF at 450 °C ($10^{-3}\,s^{-1}$)	
	Fresh	Used	Fresh	Used	Fresh	Used	Fresh	Used	Fresh	Used	Fresh	Used	Fresh	Used	Fresh	Used	Fresh	Used
SBA-15	–	–	–	–	628	–	0.97	–	7.3	–	–	–	–	–	–	–	–	–
0.5% Pd/SBA-15	5.8	5.9	–	–	563	559	0.73	0.61	6.3	6.1	26.0	25.1	55.3	53.4	2.03	2.10	13.2	10.5
0.5% Pd/5% CeO_2/SBA-15	5.6	5.7	5.4	5.4	557	551	0.86	0.56	6.1	5.9, 3.5	21.0	20.0	44.7	42.6	2.51	2.64	16.4	13.7
0.5% Pd/5% $Ce_{0.5}Zr_{0.5}O_2$/SBA-15	5.5	5.6	–	–	537	531	0.56	0.46	5.7, 3.9	5.7, 3.8	25.0	23.9	53.2	50.8	2.11	2.21	13.8	12.3
0.5% Pd/5% ZrO_2/SBA-15	5.8	6.0	–	–	577	575	0.87	0.83	6.5, 3.5	6.2, 3.4	28.2	27.3	60.0	58.1	1.87	1.94	12.2	12.6

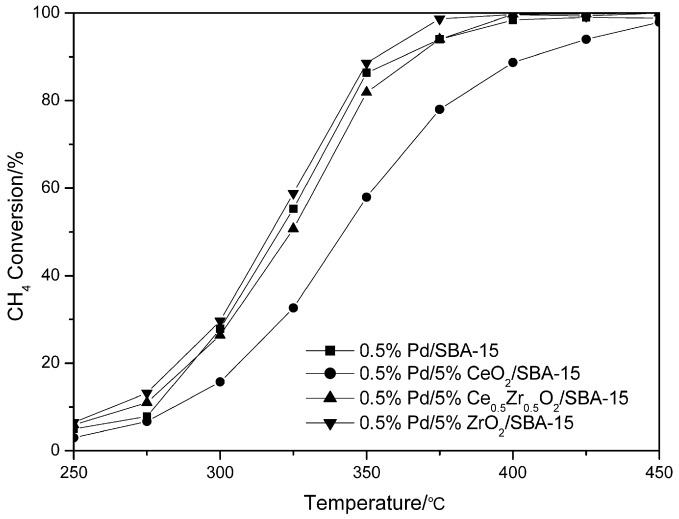

Fig. 1. Methane conversions over 0.5% Pd/SBA-15 and 0.5% Pd/5% $Ce_{1-x}Zr_xO_2$/SBA-15 catalysts.

was in the range of 16.4–12.2 × $10^{-3}\,s^{-1}$ at 450 °C, as shown in Table 2.

The observed activities of the Pd/5% $Ce_{1-x}Zr_xO_2$/SBA-15 ($x = 0$, 0.5, 1) catalysts with different Pd loadings are shown in Figs. S4–S6 in the supplementary material, and the observed activities of the 0.5% Pd/5% $Ce_{1-x}Zr_xO_2$/SBA-15 ($x = 0$, 0.5, 1) catalysts are shown in Fig. 1. The values of T_{10}, T_{50}, and T_{90} are listed in Table 1. For the Pd/5% $Ce_{1-x}Zr_xO_2$/SBA-15 ($x = 0$, 0.5, 1) catalysts, in each case the catalytic activity reached a maximum at a Pd loading of 0.75%. The TOF of the 0.5% Pd/5% CeO_2/SBA-15 catalyst was 16.4 × $10^{-3}\,s^{-1}$ at 450 °C, as shown in Table 2. From Table 1, it can be seen that for every Pd loading except 0.05%, the catalytic activity of Pd/5% CeO_2/SBA-15 was significantly worse than that of Pd/SBA-15, indicating that here CeO_2 acted as an inhibitor rather than as a promoter. Thevenin et al. [13] and Haneda et al. [8] reported that the activity of a Pd/CeO_2–Al_2O_3 catalyst in methane combustion was lower than that of a Pd/Al_2O_3 catalyst, which is consistent with our findings. At every Pd loading, the catalytic activity of Pd/5% $Ce_{1-x}Zr_xO_2$/SBA-15 increased with an increasing Zr: Ce ratio. Yue et al. [25] studied the performance of methane catalytic combustion over Pd/$Ce_xZr_{1-x}O_2$/Al_2O_3 ($x = 0$–1) catalysts and also found that the activity increased with increasing Zr content. For the catalysts with high Zr loading ($x = 0.5$ or 1), the activity was slightly greater than that of Pd/SBA-15, demonstrating that the use of $Ce_{0.5}Zr_{0.5}O_2$ or ZrO_2 improved the activity of the Pd catalysts. For Pd/5% $Ce_{1-x}Zr_xO_2$/SBA-15 ($x = 0.5$ or 1; Pd% = 0.5 or 0.75), methane could be converted completely into CO_2 and H_2O below 375 °C.

The dependence of the intrinsic activity of the 0.5% Pd/5% $Ce_{1-x}Zr_xO_2$/SBA-15 ($x = 0$, 0.5, 1) catalysts on temperature and the related Arrhenius plots are illustrated in Figs. S7 and S8, respectively. The values of T_{10}, T_{50}, and T_{90} and the activation energies are listed in Table S1. As can be seen from Table S1, the results of two runs were very close, demonstrating the high repeatability of the data. In addition, the intrinsic activity increased with decreasing activation energy. The activation energies in the range of 104–112 kJ mol^{-1} are similar to those reported previously, as shown in Table S2. For the 0.5% Pd/5% ZrO_2/SBA-15 catalyst, which had the highest intrinsic activity, methane could be completely converted to CO_2 and H_2O below 412 °C.

3.2. Catalyst stability

We chose the 0.5% Pd/5% $Ce_{1-x}Zr_xO_2$/SBA-15 and 0.5% Pd/SBA-15 catalysts to study deactivation behavior. Fig. 2 shows the results of stability tests of these catalysts. The 0.5% Pd/SBA-15 catalyst had the poorest stability. Methane conversion began to drop after 20 h on stream and was below 80% after 90 h. Incorporation of the mixed oxides $Ce_{1-x}Zr_xO_2$ ($x = 0$–1) led to a significant increase in stability in each case, with stability increasing with increasing zirconium content (x). For pure ZrO_2 ($x = 1$), the conversion of methane remained essentially complete after over 400 h on stream. To gain insight into the beneficial effect of $Ce_{1-x}Zr_xO_2$ ($x =$ 0–1) on catalyst stability of the catalyst, we investigated the properties of the catalysts before and after the stability tests by XRD, N_2 adsorption–desorption, CO chemisorption, TEM, XPS, and TPR.

3.3. XRD

Fig. 3 shows low-angle XRD patterns of the SBA-15 as support and 0.5% Pd/SBA-15 and the 0.5% Pd/5% $Ce_{1-x}Zr_xO_2$/SBA-15 ($x = 0$, 0.5, 1) catalysts before and after the stability tests. The SBA-15 support (Fig. 3a) showed three well-resolved diffraction peaks in the 2θ range 0.7–2°, corresponding to the diffraction of (100), (110),

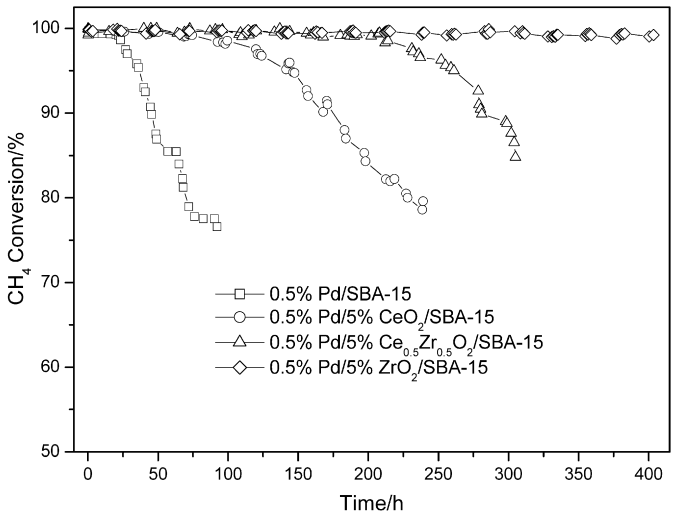

Fig. 2. Stability of the catalysts during methane combustion carried out at 450 °C.

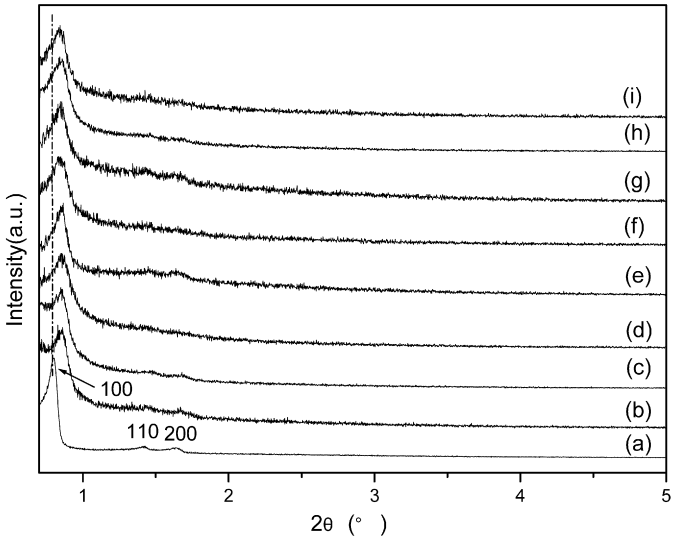

Fig. 3. Small-angle XRD patterns of SBA-15 and the catalysts before and after the stability tests: (a) SBA-15; (b) 0.5% Pd/SBA-15 (before); (c) 0.5% Pd/SBA-15 (after); (d) 0.5% Pd/5% CeO_2/SBA-15 (before); (e) 0.5% Pd/5% CeO_2/SBA-15 (after); (f) 0.5% Pd/5% $Ce_{0.5}Zr_{0.5}O_2$/SBA-15 (before); (g) 0.5% Pd/5% $Ce_{0.5}Zr_{0.5}O_2$/SBA-15 (after); (h) 0.5% Pd/5% ZrO_2/SBA-15 (before); (i) 0.5% Pd/5% ZrO_2/SBA-15 (after).

and (200) planes. These peaks are characteristic of the hexagonally ordered structure of SBA-15 [18,19]. When Pd was loaded onto SBA-15, the d_{100} peak shifted to a higher angle, and the d_{100}, d_{110}, and d_{200} peaks increased in intensity. This finding is consistent with previous reports in the literature [26]. In the Pd/SBA-15 catalysts, Pd may have been embedded into the channel of SBA-15. In this case, the d-spacing of the 100 plane would be decreased, resulting in a shift of the d_{100} peak to a higher angle. The XRD patterns of the 0.5% Pd/5% $Ce_{1-x}Zr_xO_2$/SBA-15 ($x = 0$, 0.5, 1) catalyst were essentially identical to those of the 0.5% Pd/SBA-15 catalyst. After the stability tests, the XRD patterns of these catalysts were similar to those of the fresh ones, indicating that the well-defined hexagonally ordered structure of the catalysts was not destroyed during the stability tests.

Fig. 4 shows the wide-angle XRD patterns of the catalysts before and after the stability tests. For the fresh catalysts, reflection peaks of PdO appeared, the intensities of which remained almost unchanged after incorporation of the different metal oxide phases. After the stability tests, for each catalyst, the intensity

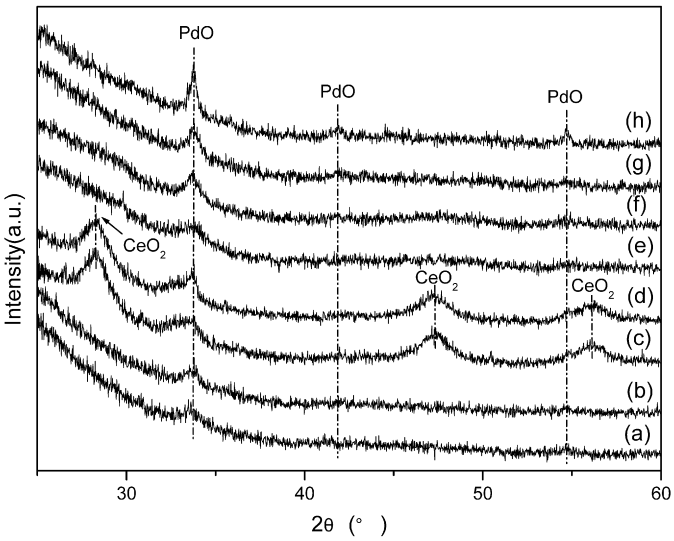

Fig. 4. Wide-angle XRD patterns of the catalysts before and after the stability tests: (a) 0.5% Pd/SBA-15 (before); (b) 0.5% Pd/SBA-15 (after); (c) 0.5% Pd/5% CeO_2/SBA-15 (before); (d) 0.5% Pd/5% CeO_2/SBA-15 (after); (e) 0.5% Pd/5% $Ce_{0.5}Zr_{0.5}O_2$/SBA-15 (before); (f) 0.5% Pd/5% $Ce_{0.5}Zr_{0.5}O_2$/SBA-15 (after); (g) 0.5% Pd/5% ZrO_2/SBA-15 (before); (h) 0.5% Pd/5% ZrO_2/SBA-15 (after).

of the PdO reflection peaks increased and the full-width-at-half-maximum (FWHM) decreased. According to the results from Scherrer's equation, the particle sizes of PdO increased slightly, as shown in Table 2; for example, for 0.5% Pd/5% CeO_2/SBA-15, PdO particle size increased from 5.6 nm to 5.7 nm. The reflection peaks of CeO_2 also appeared; their intensities remained almost unchanged, and the corresponding particle size was about 5.4 nm, suggesting no increase in the particle size of CeO_2 during reaction (Fig. 4, spectra (c) and (d)). For the 0.5% Pd/5% $Ce_{0.5}Zr_{0.5}O_2$/SBA-15 and 0.5% Pd/5% ZrO_2/SBA-15 catalysts, PdO was the only phase observed by XRD, suggesting that any $Ce_{0.5}Zr_{0.5}O_2$, CeO_2, or ZrO_2 phase had a high degree of dispersion (Fig. 4, spectra (e) and (h)). In the 0.5% Pd/5% $Ce_{0.5}Zr_{0.5}O_2$/SBA-15 catalyst, PdO particle size increased from 5.5 nm to 5.6 nm; in the 0.5% Pd/5% ZrO_2/SBA-15 catalyst, PdO particle size increased from 5.8 nm to 6.0 nm. Combining the characteristic peaks in the XRD patterns attributed to PdO and CeO_2 with the finding that the particle sizes of Pd, PdO, and CeO_2 were smaller than the pore size of SBA-15 (as shown in Table 2) confirms that they likely were incorporated into the channels of SBA-15.

3.4. N_2 adsorption–desorption and CO chemisorption measurements

Fig. 5 shows N_2 adsorption–desorption isotherms (A) and pore size distributions (B) of the various catalysts before and after stability testing and SBA-15. The textural properties of the samples are also summarized in Table 2. The isotherms of all catalysts exhibited a highly ordered mesoporous nature, whereas the sharp capillary condensation step in the range of $P/P_0 = 0.6$–0.8 attributed to the SBA-15, which has cylindrical pores with a narrow pore size distribution, disappeared. The S_{BET}, D_P, and V_P values for the fresh catalysts obviously decreased from 628 $m^2\,g^{-1}$, 7.3 nm, and 0.97 $cm^3\,g^{-1}$ for SBA-15 to no more than 577 $m^2\,g^{-1}$, 6.5 nm, and 0.87 $cm^3\,g^{-1}$, due to the incorporation of metallic Pd, its oxides, and the promoters into the SBA-15. After the stability testing, the S_{BET} and D_{BJH} values of all catalysts decreased slightly. It should be noted that the 0.5% Pd/5% ZrO_2/SBA-15 catalyst had the largest values of S_{BET} (577 $m^2\,g^{-1}$) and V_p (0.87 $cm^3\,g^{-1}$), a broad pore size distribution, and the best stability during reaction. For the 0.5% Pd/5% CeO_2/SBA-15 catalyst, the V_p value obviously de-

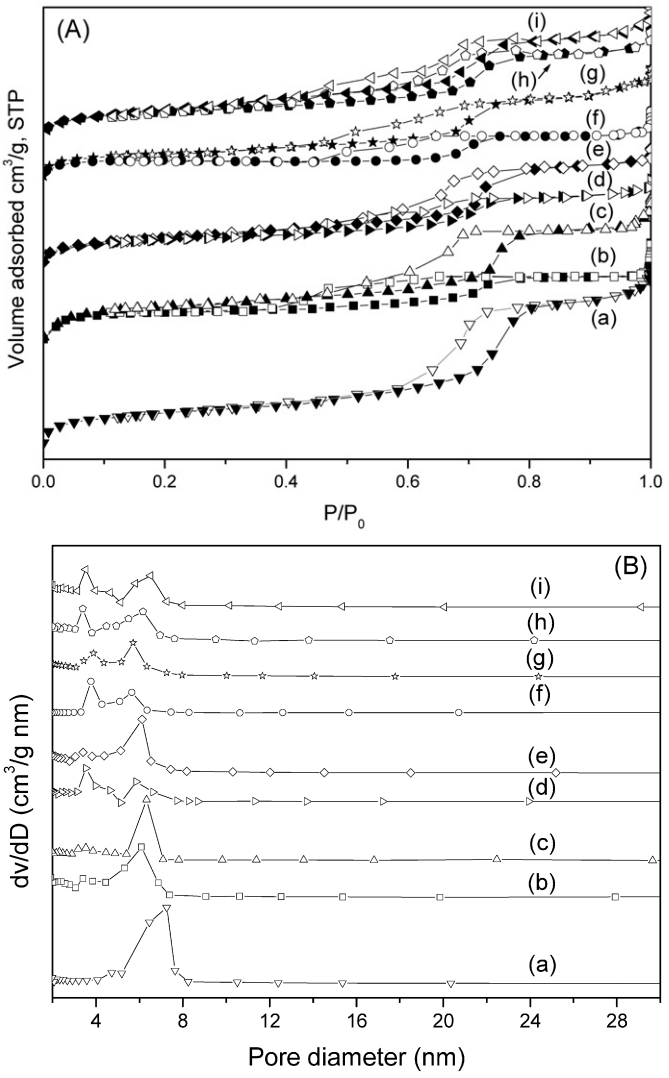

Fig. 5. N_2 adsorption–desorption isotherms (A) and pore size distributions (B) for catalyst samples before and after the stability tests: (a) SBA-15; (b) 0.5% Pd/SBA-15 (after); (c) 0.5% Pd/SBA-15 (before); (d) 0.5% Pd/5% CeO_2/SBA-15 (after); (e) 0.5% Pd/5% CeO_2/SBA-15 (before); (f) 0.5% Pd/5% $Ce_{0.5}Zr_{0.5}O_2$/SBA-15 (after); (g) 0.5% Pd/5% $Ce_{0.5}Zr_{0.5}O_2$/SBA-15 (before); (h) 0.5% Pd/5% ZrO_2/SBA-15 (after); (i) 0.5% Pd/5% ZrO_2/SBA-15 (before).

creased, from 0.86 $cm^3\,g^{-1}$ to 0.56 $cm^3\,g^{-1}$. The V_p values of other two catalysts also decreased to different extents.

Table 2 also reports the results of CO chemisorption measurements over the various catalysts before and after the stability testing. The $Ce_{1-x}Zr_xO_2$ promoters had a significant affect on Pd dispersion, Pd crystallite size, and TOF. In the fresh 0.5% Pd/5% $Ce_{1-x}Zr_xO_2$/SBA-15 ($x = 0$, 0.5, 1) catalysts, with increasing Zr content, Pd dispersion increased, whereas Pd crystallite size and TOF decreased. Compared with the corresponding fresh catalysts, in the used catalysts, dispersion decreased slightly and Pd crystallite size increased slightly. As for the TOF, except for the 0.5% Pd/5% ZrO_2/SBA-15 catalyst, the used catalysts exhibited decreased TOF compared with the corresponding fresh catalysts. The TOF in the 0.5% Pd/5% ZrO_2/SBA-15 catalyst remained almost unchanged before and after the stability tests, possibly due to the effects of ZrO_2 in promoting oxygen mobility and Pd dispersion.

3.5. TEM

Fig. 6 shows TEM micrographs of the 0.5% Pd/SBA-15 sample before and after the catalytic reaction. Fig. S9 in the supplementary material shows TEM micrographs of the 0.5% Pd/5% $Ce_{1-x}Zr_xO_2$/SBA-15 ($x = 0$, 0.5, 1) samples before and after catalytic the reaction. All samples exhibited the hexagonally ordered array of the one-dimensional mesoporous channels of SBA-15, indicating that the mesopore structure was not destroyed by the stability tests, consistent with the results of XRD and N_2 adsorption–desorption characterization. No crystallites of PdO or $Ce_{1-x}Zr_xO_2$ were found on the external surfaces, indicating that they were incorporated into the channels of the SBA-15. Moreover, the pores of the samples were open, not blocked, suggesting that the PdO and $Ce_{1-x}Zr_xO_2$ crystallites were well dispersed in all of the samples.

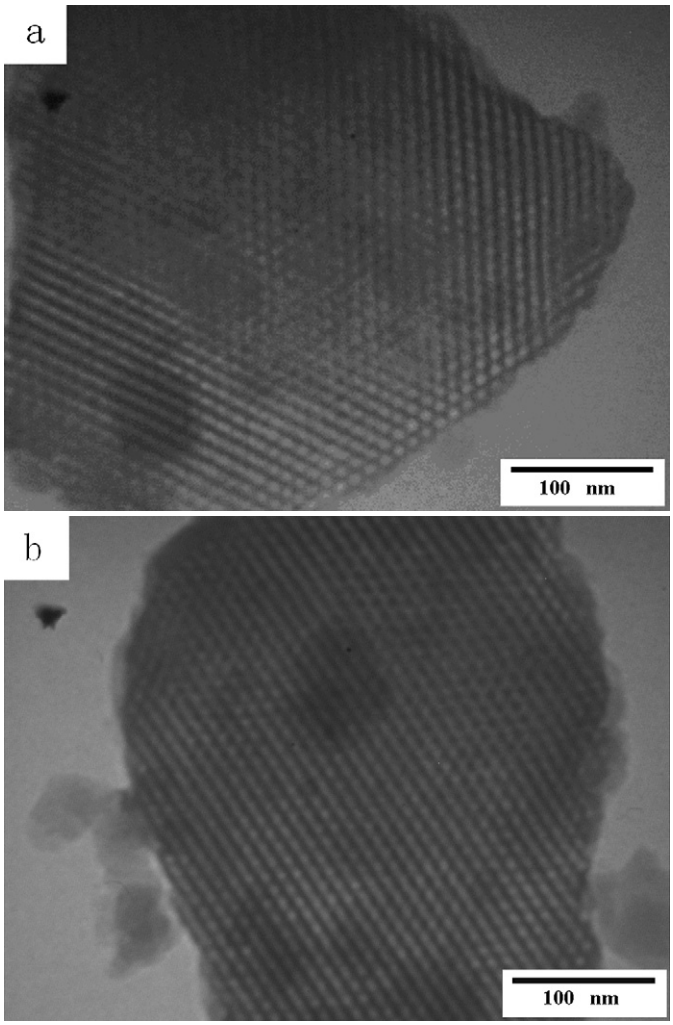

Fig. 6. TEM micrographs of 0.5% Pd/SBA-15 catalyst before and after the stability tests: (a) 0.5% Pd/SBA-15 (before); (b) 0.5% Pd/SBA-15 (after).

3.6. XPS

Table 3 gives the results of the XPS measurements. For the SBA-15 support, the measured Si/O ratio was consistent with the expected SiO_2 stoichiometry. The Si2p and O1s binding energy (BE) values of all the catalysts were very similar to those of the SBA-15 precursor and remained essentially unchanged after the stability tests. In the cerium-containing catalysts, the $Ce3d_{5/2}$ BE values and the Ce composition were very similar before and after the stability tests, respectively. For the zirconium-containing catalysts, the $Zr3d_{5/2}$ BE values of the used catalysts were essentially identical to those of the fresh catalysts, but significant changes in the composition of Zr were seen after the reaction. For the 0.5% Pd/5% $Ce_{0.5}Zr_{0.5}O_2$/SBA-15 catalyst, the amount of Zr decreased after the

Table 3
Binding energies (eV) of core electrons and surface atomic composition of samples before and after the stability tests

Samples	Si2p		O1s		$Pd3d_{5/2}$			$Ce3d_{5/2}$			$Zr3d_{5/2}$	
	BE (eV)[a]	At%	BE (eV)	At%	Pd^0 BE (eV)	Pd^{2+} BE (eV)	Pd^{4+} BE (eV)	Pd At%	BE (eV)	At%	BE (eV)	At%
SBA-15	103.4	33.34	533.0	66.66	–	–	–	–	–	–	–	–
0.5% Pd/SBA-15 (fresh)	103.3	36.56	532.9	63.31	–	337.6 (68.6)	338.5 (31.4)	0.13	–	–	–	–
0.5% Pd/SBA-15 (used)	103.4	36.11	533.0	63.78	334.7 (60.4)[b]	337.8 (23.2)	338.5 (16.4)	0.11	–	–	–	–
0.5% Pd/5% CeO_2/SBA-15 (fresh)	103.4	34.27	532.8	65.56	–	337.7 (62.7)	338.4 (37.3)	0.08	885.4	0.18	–	–
0.5% Pd/5% CeO_2/SBA-15 (used)	103.3	33.81	532.9	65.99	335.0 (57.0)	337.8 (25.8)	338.5 (17.2)	0.05	885.4	0.16	–	–
0.5% Pd/5% $Ce_{0.5}Zr_{0.5}O_2$/SBA-15 (fresh)	103.4	34.98	533.0	64.04	334.8 (25.6)	337.7 (58.1)	338.5 (16.3)	0.34	885.5	0.21	183.5	0.44
0.5% Pd/5% $Ce_{0.5}Zr_{0.5}O_2$/SBA-15 (used)	103.3	34.18	532.8	64.94	335.1 (42.0)	337.6 (45.8)	338.4 (12.2)	0.32	885.6	0.21	183.6	0.35
0.5% Pd/5% ZrO_2/SBA-15 (fresh)	103.3	37.05	533.0	61.91	335.0 (52.6)	337.7 (42.9)	338.4 (4.5)	0.42	–	–	183.3	0.62
0.5% Pd/5% ZrO_2/SBA-15 (used)	103.4	36.96	532.9	61.69	335.1 (51.9)	337.6 (43.6)	338.5 (4.5)	0.45	–	–	183.3	0.90

[a] The binding energy (BE) values were corrected using the C1s peak at 285.0 eV.
[b] The value in the brackets refers to the relative content of the components of the $Pd3d_{5/2}$ spectra.

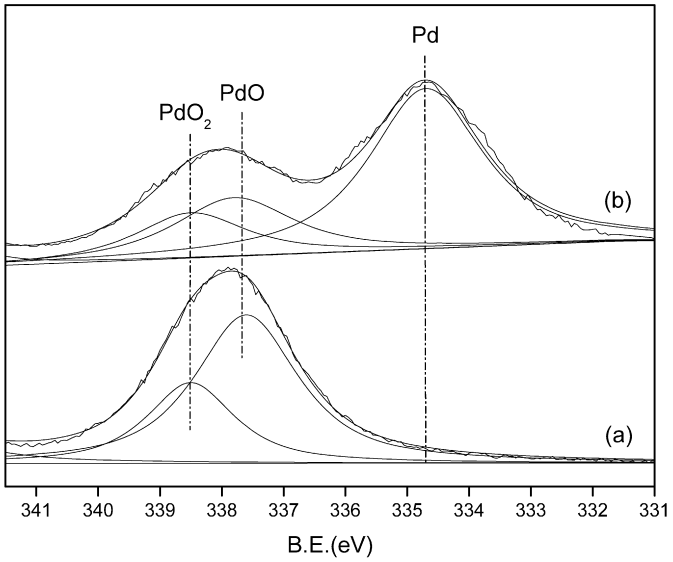

Fig. 7. XPS spectra of $Pd3d_5$ in the 0.5% Pd/SBA-15 catalyst before and after the stability tests: (a) and (b) before and after the stability tests, respectively.

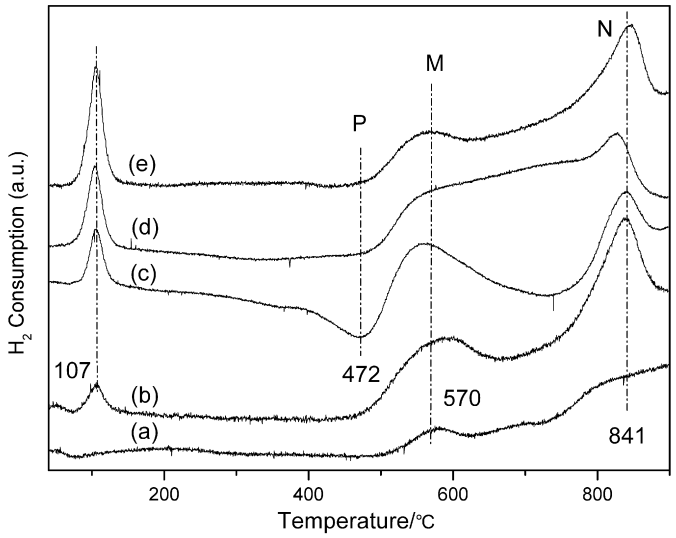

Fig. 8. TPR patterns of SBA-15 and the catalyst samples before the stability tests: (a) SBA-15; (b) 0.5% Pd/SBA-15; (c) 0.5% Pd/5% CeO_2/SBA-15; (d) 0.5% Pd/5% $Ce_{0.5}Zr_{0.5}O_2$/SBA-15; (e) 0.5% Pd/5% ZrO_2/SBA-15.

stability test, whereas for the 0.5% Pd/5% ZrO_2/SBA-15 catalyst, the amount of Zr increased markedly.

Fig. 7 shows the $Pd3d_{5/2}$ spectra of the fresh and used 0.5% Pd/SBA-15 catalysts. Figs. S10–S12 in the supplementary material show the $Pd3d_{5/2}$ spectra of the fresh and used 0.5% Pd/5% $Ce_{1-x}Zr_xO_2$/SBA-15 ($x = 0$, 0.5, 1) catalysts. Deconvolution of the $Pd3d_{5/2}$ spectra suggests that except for the fresh Pd/SBA-15 and fresh Pd/CeO_2/SBA-15, in general there were three components with $Pd3d_{5/2}$ BE values of 334.7–335.1 eV, 337.6–337.8 eV, and 338.4–338.5 eV, which remained almost unchanged after the stability tests. These can be attributed to Pd^0 [27], Pd^{2+} [28–30], and Pd^{4+} [31], respectively.

As shown in Table 3, although the total Pd content of each catalyst was the same and remained almost unchanged before and after the stability tests, significant changes occurred in the relative amounts of Pd^0, Pd^{2+}, and Pd^{4+}. For the fresh 0.5% Pd/SBA-15 (Fig. 7) and 0.5% Pd/5% CeO_2/SBA-15 (Fig. S10) catalysts, no Pd^0 was present, but after the stability tests, Pd^0 was the predominant species (ca. 60%) in both cases. The 0.5% Pd/5% $Ce_{0.5}Zr_{0.5}O_2$/SBA-15 catalyst also exhibited a significantly increased amount of Pd^0 after the stability tests (Fig. S11). In contrast, for the 0.5% Pd/5% ZrO_2/SBA-15 catalyst, the relative amounts of Pd^0, Pd^{2+}, and Pd^{4+} remained almost unchanged after the stability tests (Fig. S12).

3.7. TPR measurements

Fig. 8 shows the results of TPR measurements on the samples before the stability tests. For the SBA-15 support, a weak reduction peak occurred at about 570 °C, designated M, attributed to condensation reactions between the surface silanol groups of mesoporous silica and the metal source during heat treatment [32]. In addition, a broad peak at about 841 °C, designated N, was seen on further condensation reactions at high temperature. For the 0.5% Pd/SBA-15 catalyst, an additional weak peak due to reduction of PdO was seen at about 107 °C [33]. The positions of the M and N peaks were essentially the same as those of the SBA-15, but their areas were increased, probably because the addition of Pd enhanced the condensation reactions. When CeO_2 was added, the reduction temperature of PdO remained constant, but its area increased significantly, indicating that adding CeO_2 affected the redox properties of PdO. The temperatures of the M and N peaks also remained almost unchanged, but their areas became slightly larger than those for 0.5% Pd/SBA-15. There also was a negative reduction peak, designated P, which can be attributed to the decomposition of cerium hydride. This phenomenon likely occurs in the lanthanide oxides due to H_2 treatment; for example, Jujjuri et al. [34] reported that lanthanides can form hydrides (LnH_2/LnH_3, Ln = La, Ce, Sm, Eu, Gd, and Yb) on contact with H_2 at room temperature. Thus, the negative reduction peak P in the TPR of the 0.5% Pd/5% CeO_2/SBA-15 catalyst is likely due to the decomposition of cerium hydride. In the presence of $Ce_{0.5}Zr_{0.5}O_2$ or ZrO_2, even though the reduction temperature of PdO remained almost unchanged, its area increased relative to that of 0.5% Pd/SBA-15 or 0.5% Pd/5% CeO_2/SBA-15. The reduction temperatures of the M and N also remained almost unchanged, but their areas de-

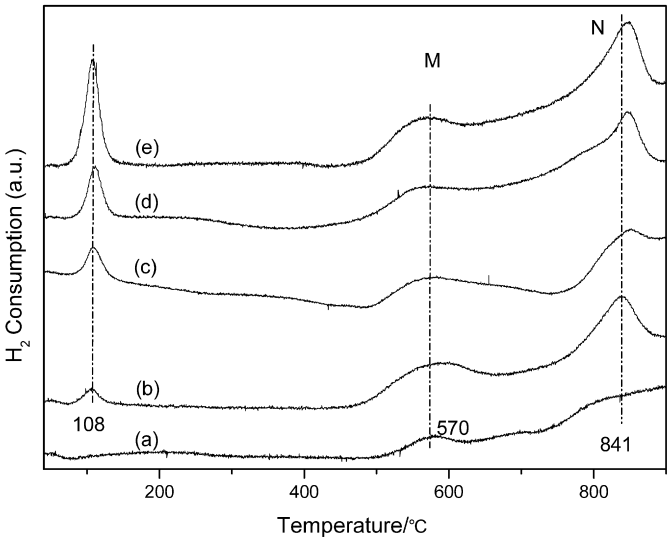

Fig. 9. TPR patterns of SBA-15 and the samples after the stability tests: (a) SBA-15; (b) 0.5% Pd/SBA-15; (c) 0.5% Pd/5% CeO_2/SBA-15; (d) 0.5% Pd/5% $Ce_{0.5}Zr_{0.5}O_2$/SBA-15; (e) 0.5% Pd/5% ZrO_2/SBA-15.

creased slightly. The negative reduction peak disappeared in the two catalysts. In the 0.5% Pd/5% $Ce_{0.5}Zr_{0.5}O_2$/SBA-15 catalyst, Zr likely prevented Ce from forming cerium hydride, due to the strong interaction between Zr and Ce [35].

Fig. 9 shows the results of TPR measurements on the samples after the stability tests. Comparing this figure with Fig. 8 shows some significant differences in redox properties between the fresh and used catalyst samples. For 0.5% Pd/SBA-15 and 0.5% Pd/5% CeO_2/SBA-15, the reduction temperatures of PdO remained almost unchanged after the stability tests, but the area decreased significantly in each case, indicating a drop in H_2 consumption during PdO reduction. The reduction temperatures of the M and N peaks also were almost unchanged, and the peak areas decreased slightly. For 0.5% Pd/5% $Ce_{0.5}Zr_{0.5}O_2$/SBA-15, the reduction temperature of the PdO peak remained unchanged after the stability test but the peak area decreased, again indicating a drop in H_2 consumption during PdO reduction. After the catalyst tests, the M peak's temperature was unchanged but its area decreased, whereas the N peak shifted to a slightly higher temperature and its area increased. In contrast, for 0.5% Pd/5% ZrO_2/SBA-15, the reduction temperatures and areas of the PdO peak were essentially identical for the fresh and used catalysts, indicating no change in H_2 consumption during PdO reduction. The reduction temperatures and areas of the M and N peaks also were very similar before and after the stability tests.

4. Discussion

There is some controversy in the literature as to the identity of the active phase in the oxidation of methane catalyzed by palladium—Pd, PdO, or a mixed Pd^0/PdO phase. Most investigators have concluded that PdO is active in methane combustion, whereas metallic palladium is inactive [3–5,36–38]. For the mixed-phase Pd^0/PdO, many consider the active form to be PdO; however, the presence of Pd^0 can increase the catalyst activity by providing more active sites for the dissociation of methane, which allows the overall reaction to proceed more rapidly [16,39]. In our case, Pd^0 was not present in the 0.5% Pd/SBA-15 and 0.5% Pd/5% CeO_2/SBA-15 catalysts (as shown in Table 3) even though these two catalysts demonstrated higher activity, suggesting that PdO was the active phase.

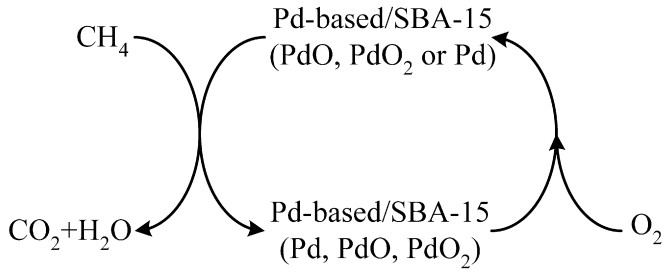

Fig. 10. The redox processes of Pd-based SBA-15 catalysts for the catalytic combustion of methane.

Although some studies of the deactivation behavior of Pd-based catalysts for the catalytic combustion of methane have been published [7–11,40], the phenomenon remains incompletely understood. It has been suggested that the major factors leading to catalyst deactivation are support sintering, growth of PdO and/or Pd particles, and transformation of PdO to Pd, depending on the properties of the support and the promoter, the catalysts preparation method, and the reaction conditions.

The results of XRD, N_2 adsorption–desorption, and TEM characterization show that although the incorporation of PdO and $Ce_{1-x}Zr_xO_2$ into the channels of SBA-15 produced some changes in the textural properties of the catalysts, the catalysts still retained the mesopore structure of SBA-15 before and after the stability tests. Thus, clearly deactivation of the catalysts cannot be ascribed to sintering or degradation of the SBA-15 support.

The XRD and CO chemisorption studies confirm that although all of the catalysts demonstrated a slight increase in PdO particle size and a decrease in Pd dispersion during the reaction, the Pd/SBA-15, 0.5% Pd/5% CeO_2/SBA-15 and 0.5% Pd/5% $Ce_{0.5}Zr_{0.5}O_2$/SBA-15 catalysts deactivated to very different extents, whereas the 0.5% Pd/5% ZrO_2/SBA-15 catalyst exhibited no deactivation, suggesting that the growth of PdO particles likely was not the major factor responsible for the catalyst deactivation.

It is generally accepted that Pd-catalyzed combustion of methane occurs by a redox mechanism [17,35,41–43]. According to this mechanism, PdO is reduced to Pd by methane, producing H_2O and CO_2, and Pd is reoxidized to PdO by oxygen. In an early study of Pd/Al_2O_3 catalyst, Farrauto et al. [36] found that although the PdO–Pd transformation was reversible, Pd could not be completely reoxidized. For the same system, Su et al. [44] also found that the small Pd particles formed in the reduction became separated from the surface of the PdO and could not be fully reoxidized to PdO due to the limited diffusion of oxygen, resulting in the nucleation and growth of Pd particles, which deactivated the catalyst. Obviously, in a multicomponent solid-phase system comprising Pd, PdO, and PdO_2 in which PdO is the active phase, the deactivation behavior of the Pd-based catalyst is closely related to the stability of its phases, which in turn strongly depends on the redox properties of the catalyst and the reaction conditions. It is well known that oxygen diffusion plays a very important role in determining the redox properties of solid catalysts, and is related to their oxygen storage capacity, oxygen mobility, and dispersion of promoters and the phases involved in the activity. Fig. 10 illustrates possible reaction mechanisms for catalysis of methane combustion over the 0.5% Pd/SBA-15 and 0.5% Pd/5% $Ce_{1-x}Zr_xO_2$/SBA-15 ($x = 0$, 0.5, 1) catalysts. The OSC and oxygen mobility of the support varied with the identity of the metal oxide promoter $Ce_{1-x}Zr_xO_2$. Accordingly, the reaction mechanism can be analyzed by studying the influence of the promoter on the OSC and the oxygen mobility of the support.

Connecting the foregoing analysis with our cases, based on the XPS, CO chemisorption, and TPR findings, in the 0.5% Pd/SBA-15 catalyst, only PdO and PdO_2 were initially present, with no Pd^0 (Ta-

ble 3). Because PdO_2 is known to readily reduce to PdO and then to Pd [45], we propose that both PdO and PdO_2 were reduced to Pd by CH_4, and Pd was reoxidized to PdO and PdO_2 by O_2. The redox processes involving PdO_2/PdO and Pd were not in equilibrium. The oxygen consumed in the reaction process could not be replenished fast enough by migration of oxygen from the gas phase. The reoxidation of Pd^0 was retarded, and Pd^0 accumulated gradually (Table 3), resulting in decreased TOF (Table 2) due to deterioration of the redox properties (Figs. 8 and 9), and catalyst deactivation after about 20 h on stream (Fig. 2).

Farrauto et al. [46] studied the effect of CeO_2 on the equilibration of PdO–Pd and found that CeO_2 could enhance the reoxidation of Pd. Thevenin et al. [13] studied various catalysts modified with CeO_2 and also confirmed that CeO_2 could increase the rate of Pd reoxidation. These authors suggested that CeO_2 has high OSC and oxygen mobility and can provide oxygen rapidly, accelerating the reoxidation of Pd. But although the 0.5% Pd/5% CeO_2/SBA-15 catalyst was somewhat more stable than the 0.5% Pd/SBA-15 catalyst (as shown in Fig. 2), methane conversion over this catalyst still began to decrease after about 96 h on stream. Furthermore, the deactivated catalyst contained large amounts of Pd^0 (Table 3), suggesting that the equilibration between PdO/PdO_2 and Pd^0 was not maintained.

These findings demonstrated that although the OSC and oxygen mobility of the catalyst were increased by the addition of CeO_2, the effect was limited. Di Monte et al. [14] and Fornasiero et al. [47] found that CeO_2 sintered readily on heat treatment, after which its OSC decreased markedly. Fig. 4 shows diffraction peaks of CeO_2 for the 0.5% Pd/5% CeO_2/SBA-15 catalyst, suggesting that sintering of CeO_2 likely occurred after heat treatment, resulting in the growth of CeO_2 particles and a concomitant decrease in OSC. At the same time, the CeO_2 dispersion decreased due to particle growth and, as a result, the rate of oxygen exchange between CeO_2 and PdO/PdO_2 and the gas phase decreased, inducing transformation of PdO to Pd (Table 3) and a decrease in TOF (Table 2) due to deterioration of the redox properties (Figs. 8 and 9). Therefore, the 0.5% Pd/5% CeO_2/SBA-15 became deactivated after a relatively short time.

As is well known, insertion of ZrO_2 into cubic CeO_2 results in increased OSC, which improves the activity and thermal stability of catalysts. Distortion of the O^{2-} sublattice in the mixed oxide permits greater mobility of the lattice oxygen species [48,49], with reduction no longer confined to the surface but extending into the bulk [47,50]. It has been reported that the percentage of reducible Ce^{4+} and the thermal stability increase with increasing Zr/Ce ratio, and that insertion of Zr results in maintenance of a high degree of dispersion at relatively high temperatures, which increases oxygen mobility [51]. As shown in Fig. 2, the 0.5% Pd/5% $Ce_{0.5}Zr_{0.5}O_2$/SBA-15 was more stable than the 0.5% Pd/5% CeO_2/SBA-15, but methane conversion began to decrease after about 315 h on stream. Furthermore, the deactivated catalyst had more Pd^0 and less PdO_2 and PdO (Table 3) compared with the fresh sample, suggesting that the redox equilibration between PdO_2/PdO and Pd^0 remained perturbed during the stability tests. Although the CeO_2–ZrO_2 mixed oxide had a higher OSC than the CeO_2 [51], and the presence of $Ce_{0.5}Zr_{0.5}O_2$ led to an increase in the OSC and oxygen mobility of the catalyst, these increases were not sufficient to prevent an oxygen deficiency and an eventual Pd^0 buildup, eventually resulting in catalyst deactivation.

For the 0.5% Pd/5% ZrO_2/SBA-15 catalyst, no deactivation was seen after more than 400 h on stream (Fig. 2). Moreover, the relative amounts of Pd^0, Pd^{2+}, and Pd^{4+} (Table 3); the redox property of the catalyst (Figs. 8 and 9); and the TOFs (Table 2) remained essentially unchanged after the reaction, suggesting that the high OSC and good oxygen mobility of the catalyst with ZrO_2 as the promoter maintained a high oxidation state of Pd even though this catalyst had the greatest degree of Pd dispersion. Ciuparu et al. [52], studying the oxygen exchange between Pd and ZrO_2, found that ZrO_2 exhibited high rates of oxygen exchange and oxygen mobility due to the presence of surface oxygen vacancies, which facilitate the oxygen exchange between the bulk phase and the surface. This finding explains the results of this study of the deactivation behavior of the 0.5% Pd/5% ZrO_2/SBA-15 catalyst.

5. Conclusion

Catalysts based on Pd/SBA-15 showed excellent activity for the catalytic combustion of methane, in which a palladium loading of 1% gave maximum observed activity with a T_{90} value of 354 °C. Although the Pd/SBA-15 catalysts exhibited high initial activity, they showed very poor stability. Using $Ce_{1-x}Zr_xO_2$ as a promoter improved the stability of the catalysts. The optimum $Ce_{1-x}Zr_xO_2$ loading was 5%. In the series of 0.5% Pd/5% $Ce_{1-x}Zr_xO_2$/SBA-15 catalysts, both the activity and stability were found to increase with increasing Zr content (x). The 0.5% Pd/5% ZrO_2/SBA-15 catalyst exhibited the highest activity and stability of all catalysts studied. The methane conversion remained unchanged after 400 h at 450 °C.

The 0.5% Pd/SBA-15 and 0.5% Pd/5% $Ce_{1-x}Zr_xO_2$/SBA-15 ($x = 0$, 0.5, 1) catalysts retained the hexagonally ordered structure of the SBA-15 before and after the stability tests. PdO particles were formed in the channels of SBA-15 and increased slightly in size during the reaction, but this was not the major cause of the loss of catalyst activity. Catalyst stability was seen to depend mainly on the OSC and oxygen mobility, and the deactivation behavior can be interpreted in terms of the redox mechanism. For all of the catalysts studied except 0.5% Pd/5% ZrO_2/SBA-15, the redox equilibration between Pd and PdO_2/PdO was perturbed during the reaction due to a limited oxygen-transfer ability, resulting in the transformation of PdO to Pd and leading to catalyst deactivation. In the 0.5% Pd/5% ZrO_2/SBA-15 catalyst, the high OSC and oxygen mobility with ZrO_2 as a promoter allowed more rapid transfer of oxygen to Pd during the stability tests, and thus the catalyst exhibited stable TOF and the best stability.

Acknowledgments

Financial support for this work was provided by the National Natural Science Foundation of China (project 20473009), National 863 Project (2006AA10Z425) and the National Basic Research Program of China (project 2005CB221405).

Supplementary material

The online version of this article contains additional supplementary material.

Please visit DOI: 10.1016/j.jcat.2008.04.010.

References

[1] D. Ciuparu, M.R. Lyubovsky, E. Altman, L.D. Pfefferle, A. Datye, Catal. Rev. 44 (2002) 593.
[2] P. Gélin, M. Primet, Appl. Catal. B 39 (2002) 1.
[3] C.F. Cullis, B.M. Willatt, J. Catal. 83 (1983) 267.
[4] P.O. Thevenin, E. Pocoroba, L.J. Pettersson, H. Karhu, I.J. Vayrynen, S.G. Jaras, J. Catal. 207 (2002) 139.
[5] B. Kucharczyk, W. Tylus, L. Kepinski, Appl. Catal. B 49 (2004) 27.
[6] H. Yoshida, T. Nakajima, Y. Yazawa, T. Hattori, Appl. Catal. B 71 (2007) 70.
[7] H. Arai, M. Machida, Catal. Today 10 (1991) 81.
[8] M. Haneda, T. Mizushima, N. Kakuta, J. Phys. Chem. B 102 (1998) 6579.
[9] Y. Ozawa, Y. Tochihara, M. Nagai, S. Omi, Chem. Eng. Sci. 58 (2003) 671.
[10] Y. Ozawa, Y. Tochihara, A. Watanabe, M. Nagai, S. Omi, Appl. Catal. A 259 (2004) 1.
[11] P. Euzen, J.H.L. Gal, B. Rebours, G. Martin, Catal. Today 47 (1999) 19.
[12] Y.Q. Deng, T.G. Nevell, Catal. Today 47 (1999) 279.

[13] P.O. Thevenin, A. Alcalde, L.J. Pettersson, S.G. Järås, J.L.G. Fierro, J. Catal. 215 (2003) 78.
[14] R. Di Monte, P. Fornasiero, J. Kašpar, P. Rumori, G. Gubitosa, M. Graziani, Appl. Catal. B 24 (2000) 157.
[15] P. Fornasiero, R. Di Monte, G. Rsga Rao, J. Kaspar, S. Meriani, A. Trovarelli, M. Graziani, J. Catal. 151 (1995) 168.
[16] W.S. Epling, G.B. Hoflund, J. Catal. 182 (1999) 5.
[17] C.A. Müller, M. Maciejewski, R.A. Koeppel, A. Baiker, Catal. Today 47 (1999) 245.
[18] D. Zhao, J. Feng, Q. Huo, N. Melosh, G.H. Fredrickson, B.F. Chmelka, G.D. Stucky, Science 279 (1998) 548.
[19] M. Hartmann, A. Vinu, Langmuir 18 (2002) 8010.
[20] I. Yuranov, P. Moeckli, E. Suvorova, P. Buffat, L. Kiwi-Minsker, A. Renken, J. Mol. Catal. A 192 (2003) 239.
[21] I. Yuranov, L. Kiwi-Minsker, A. Renken, Appl. Catal. B 43 (2003) 217.
[22] L. Li, J.L. Shi, J.N. Yan, Chem. Commun. (2004) 1990.
[23] L. Li, L.X. Zhang, J.L. Shi, J.N. Yan, J. Liang, Appl. Catal. A 283 (2005) 85.
[24] S.S. Lee, H.I. Park, B.K. Park, S.H. Byeon, Mater. Sci. Eng. B 135 (2006) 20.
[25] B.H. Yue, R.X. Zhou, Y.J. Wang, X.X. Han, X.M. Zheng, Appl. Surf. Sci. 246 (2005) 36.
[26] P. Han, X. Wang, X. Qiu, X. Ji, L. Gao, J. Mol. Catal. A 272 (2007) 136.
[27] N. Ikeo, Y. Iijima, N. Nimura, M. Sigematsu, T. Tazawa, S. Matsumoto, K. Kojima, Y. Nagasawa, Handbook of X-Ray Photoelectron Spectroscopy, JEOL, Tokyo, 1991.
[28] L.H. Xiao, K.P. Sun, X.L. Xu, X.N. Li, Catal. Commun. 6 (2005) 796.
[29] L.M.T. Simplício, S.T. Brandão, E.A. Sales, L. Lietti, F. Bozon-Verduraz, Appl. Catal. B 63 (2006) 9.
[30] E.H. Voogt, A.J.M. Mens, O.L.J. Gijzeman, J.W. Geus, Surf. Sci. 350 (1996) 21.
[31] K. Otto, L.P. Haack, J.E. deVries, Appl. Catal. B 1 (1992) 1.
[32] Y. Park, T. Kang, P. Kim, J. Yi, J. Colloid Interface Sci. 295 (2006) 464.
[33] Y. Liu, T. Hayakawa, T. Ishii, M. Kumagai, H. Yasuda, K. Suzuki, S. Hamakawa, K. Murata, Appl. Catal. A 210 (2001) 301.
[34] S. Jujjuri, E. Ding, S.G. Shore, M.A. Keane, J. Mol. Catal. A 272 (2007) 96.
[35] S. Damyanova, B. Pawelec, K. Arishtirova, M.V.M. Huerta, J.L.G. Fierro, Appl. Catal. A 337 (2008) 86.
[36] R.J. Farrauto, M.C. Hobson, T. Kennelly, E.M. Waterman, Appl. Catal. A 81 (1992) 227.
[37] K. Sekizawa, M. Machida, K. Eguchi, H. Arai, J. Catal. 142 (1993) 655.
[38] R. Burch, F.J. Urbano, Appl. Catal. A 124 (1995) 121.
[39] J.N. Carstens, S.C. Su, A.T. Bell, J. Catal. 176 (1998) 136.
[40] A.K. Neyestanaki, F. Klingstedt, T. Salmi, D.Y. Murzin, Fuel 83 (2004) 395.
[41] K.I. Fujimoto, F.H. Riberio, M. Avalos-Borja, E. Iglesia, J. Catal. 179 (2) (1998) 431.
[42] C.A. Mueller, M. Maciejewski, R.A. Koeppel, R. Tschan, A. Baiker, J. Phys. Chem. 100 (5) (1996) 20006.
[43] C.A. Mueller, M. Maciejewski, R.A. Koeppel, A. Baiker, J. Catal. 166 (1) (1997) 36.
[44] S.C. Su, J.N. Carstens, A.T. Bell, J. Catal. 176 (1998) 125.
[45] J.G. McCarty, Catal. Today 26 (1995) 283.
[46] R.J. Farrauto, J.K. Lampert, M.C. Hobson, E.M. Waterman, Appl. Catal. B 6 (1995) 263.
[47] P. Fornasiero, G. Balducci, R. Di Monte, J. Kaspar, V. Sergo, G. Gubitosa, A. Ferrero, M. Graziani, J. Catal. 164 (1996) 173.
[48] P. Fornasiero, E. Fonda, R. Di Monte, G. Vlaic, J. Kaspar, M. Graziani, J. Catal. 187 (1999) 177.
[49] G. Vlaic, P. Fornasiero, S. Geremia, J. Kaspar, M. Graziani, J. Catal. 168 (1997) 386.
[50] A. Trovarelli, F. Zamar, J. Llorca, C. de Leitenburg, G. Dolcetti, J.T. Kiss, J. Catal. 169 (1997) 490.
[51] C.E. Hori, H. Permana, K.Y.S. Ng, A. Brenner, K. More, K.M. Rahmoeller, D. Belton, Appl. Catal. B 16 (1998) 105.
[52] D. Ciuparu, F. Bozon-Verduraz, L. Pfefferle, J. Phys. Chem. B 106 (2002) 3434.